NeuroImage 182 (2018) 479–487

Contents lists available at ScienceDirect

NeuroImage

journal homepage: www.elsevier.com/locate/neuroimage

High resolution in-vivo diffusion imaging of the human hippocampus

Sarah Treit [a], Trevor Steve [b], Donald W. Gross [b], Christian Beaulieu [a,*]

[a] Department of Biomedical Engineering, Faculty of Medicine & Dentistry, University of Alberta, Canada
[b] Division of Neurology, Faculty of Medicine & Dentistry, University of Alberta, Canada

ARTICLE INFO

Keywords:
Diffusion acquisition
Hippocampal subfields
Diffusion tensor imaging
DTI
Cornu ammonis
CA
Dentate gyrus
Stratum lacunosum moleculare
SLM

ABSTRACT

The human hippocampus is a key target of many imaging studies given its capacity for neurogenesis, role in long term potentiation and memory, and nearly ubiquitous involvement in neurological and psychiatric conditions. Diffusion tensor imaging (DTI) has detected microstructural abnormalities of the human hippocampus associated with various disorders, but acquisitions have typically been limited to low spatial resolution protocols designed for whole brain (e.g. >2 mm isotropic, >8 mm^3 voxels), limiting regional specificity and worsening partial volume effects. The purpose here was to develop a simple DTI protocol using readily available standard single-shot EPI at 3T, capable of yielding much higher spatial resolution images (1 x 1 x 1 mm^3) of the human hippocampus in a 'clinically feasible' scan time of ~6 min. A thin slab of twenty 1 mm slices oriented along the long axis of the hippocampus enabled efficient coverage and a shorter repetition time, allowing more diffusion weighted images (DWIs) per slice per unit time. In combination with this strategy, a low b value of 500 s/mm^2 was chosen to help overcome the very low SNR of a 1 x 1 x 1 mm^3 EPI acquisition. 1 mm isotropic mean DWIs (averaged over 120–128 DWIs) showed excellent detail of the hippocampal architecture (e.g. morphology and digitations, subregions, stratum lacunosum moleculare - SLM) that was not readily visible on 2 mm isotropic diffusion images. Diffusion parameters within the hippocampus were consistent across subjects and fairly homogenous across subregions of the hippocampus (with the exception of the SLM and tail). However, it is expected that DTI parameters will be sensitive to microstructural changes associated with a number of clinical disorders (e.g. epilepsy, dementia) and that this practical, translatable approach for high resolution acquisition will facilitate localized detection of hippocampal pathology.

Introduction

Ultra-high resolution *ex-vivo* diffusion tensor imaging (DTI) of the 'healthy' human hippocampus yields diffusion-weighted images and colour anisotropy maps which enable visualization of internal architecture variations of fractional anisotropy (FA) and mean diffusivity (MD) reflecting known microstructural heterogeneity identified with histology (Shepherd et al., 2007). Further, e*x-vivo* DTI of hippocampal sclerosis in temporal lobe epilepsy patients (i.e. samples from hippocampal resection aimed to control seizures) has demonstrated aberrant intra-hippocampal connections (Modo et al., 2016), reduced layers (Coras et al., 2014), and microstructural variation reflecting changes in neuronal cell bodies, dendritic fields, and axonal projection systems (Colon-Perez et al., 2015) confirmed with histology in these same samples. The ultra-high spatial resolution (60–220 μm in-plane with 0.1–0.7 mm thick slices; 0.001–0.011 mm^3 voxel volumes) of these *ex-vivo* datasets is made possible by high field strengths (7–17.6 T), small RF coils with increased sensitivity, and very long scan times (5–15 h).

Given its demonstrated utility *ex-vivo*, there is significant interest in *in-vivo* diffusion imaging of the hippocampus, which may provide unique information about regional microstructural pathology that precedes or coincides with macrostructural changes such as volume loss typically quantified on conventional high-resolution relaxation-weighted scans in a variety of disorders. A number of previous studies have demonstrated DTI changes in the hippocampus associated with aging (e.g. Cherubini et al., 2009; Yassa et al., 2011), mild cognitive impairment and dementia (e.g. Li et al., 2013; Tang et al., 2016; van Uden et al., 2016), epilepsy (Nazem-Zadeh et al., 2014), ALS (Barbagallo et al., 2014), multiple sclerosis (Cappellani et al., 2014; Planche et al., 2017), stroke (Kliper et al., 2016), schizophrenia (Chiapponi et al., 2014; Nazeri et al., 2017) and others. Interestingly, diffusion parameters have also been shown to be sensitive to transient, short-time scale changes in hippocampal microstructure correlating with various processes in healthy adults, including learning and memory (Sagi et al., 2012) and sex hormone

* Corresponding author. 1098 Research Transition Facility, Department of Biomedical Engineering, University of Alberta, Edmonton T6G-2V2, AB, Canada.
E-mail address: christian.beaulieu@ualberta.ca (C. Beaulieu).

https://doi.org/10.1016/j.neuroimage.2018.01.034
Received 24 August 2017; Accepted 15 January 2018
Available online 1 February 2018
1053-8119/

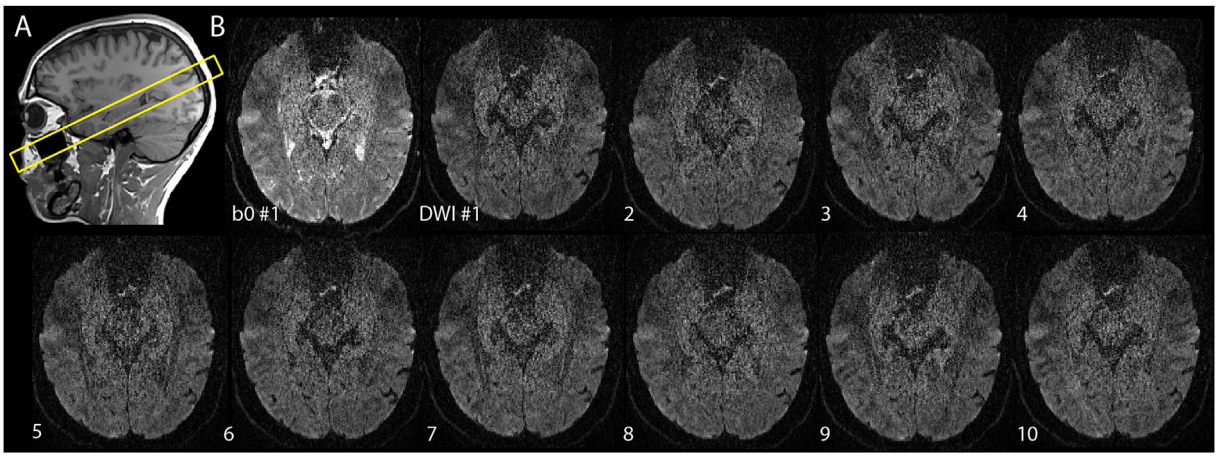

Fig. 1. (A) A slab of twenty 1 mm axial oblique slices aligned along the long axis of the hippocampus was acquired to reduce scan time and limit coverage to just the hippocampus, as prescribed on a sagittal slice of the 3D T1-weighted MPRAGE. (B) Examples of individual images, including 1 b = 0 s/mm^2 and 10 unique gradient directions at 500 s/mm^2. It is visually evident that despite signal boosting strategies, acquisition of 1 x 1 x 1 mm^3 resolution produces very low signal-to-noise images (~3–5 in the hippocampus). Note that pre-scan normalize was used to minimize B1 sensitivity variations across the slice and improve visualization of the hippocampus.

fluctuations in the female menstrual cycle (Barth et al., 2016). This work collectively suggests that diffusion tensor parameters are sensitive, albeit not specific, to microstructural change in the hippocampus over a wide range of conditions and disorders. However, these studies have almost exclusively used whole-brain diffusion protocols with poor spatial resolution (i.e. ≥ 2 mm isotropic) and have extracted diffusion values either from a manually drawn single-slice region of interest, or averaged across the whole hippocampus as delineated on co-registered anatomical images such as T1.

Down-sampling of *ex-vivo* DTI acquisitions demonstrates that despite the obvious increase in partial volume effects relative to 0.1 or even 0.5 mm^3, 1 mm^3 resolution provides marked improvement in delineation of hippocampal structures relative to the 8 mm^3 typical of most currently published *in-vivo* studies (see MD maps in Fig. 4 of Modo et al., 2016). Although another *ex-vivo* study conversely concluded that down-sampling of 220 μm ex-vivo images to 1 mm^3 was insufficient to delineate internal structures (Colon-Perez et al., 2015), it should be noted that this study examined tissue samples from hippocampal sclerosis, which is itself characterized by a loss of internal architecture (Jackson et al., 1993). The utility of 1 mm isotropic resolution in the healthy human hippocampus should therefore be evaluated *in vivo* in order to determine any advantage over a standard DTI acquisition of ~2 mm isotropic (8 mm^3 voxel volume). Specifically, in addition to allowing for visual discrimination of structure on diffusion images, this resolution could potentially mitigate the need for co-registration to anatomical images, thus greatly improving accuracy and reducing partial volume effects on diffusion parameters.

Beyond whole hippocampus measurements, there is also significant interest in imaging hippocampal sub-fields, which play unique roles in human memory (Neunuebel and Knierim, 2014) and the pathophysiology of several diseases (e.g. Epilepsy, Steve et al., 2014; and Alzheimer's Disease, West et al., 1994). A few papers have reported diffusion parameters within hippocampal subfields by delineating on T1 or T2 and then co-registering with DTI maps. While this work has suggested sub-field specific associations between diffusion parameters and aging (Pereira et al., 2014), epilepsy sub-types (Bernhardt et al., 2016), anxiety and depression (Cha et al., 2016), and memory (Kobe et al., 2016), these DTI acquisitions used low spatial resolutions of 2–2.5 mm isotropic or $1.7 \times 1.7 \times 3$ mm^3 (8–15.6 mm^3 voxels), leading to concerns with accuracy and partial volume effects which may be mitigated at higher spatial resolutions. Multi-shot EPI with a spatial resolution of 1.4 mm isotropic has demonstrated the potential for high resolution diffusion imaging of the human hippocampus and its white matter circuitry *in vivo*, but the method required a clinically infeasible scan time of 60 min (8.5 min x 7 repetitions for 70 directions at 1500 s/mm^2) even for limited coverage of 27 slices at 3T with an 8 channel RF coil (Zeineh et al., 2012).

The purpose of this study was to develop and test a practical acquisition using single-shot 2D EPI that could yield high quality 1 mm isotropic resolution *in-vivo* diffusion tensor images of the human hippocampus within a 'clinically feasible' scan time of ~6 min at 3T. The protocol proposed here can be readily translated to other sites given its use of standard methodology and efficient scan time allowing it to be incorporated with other key scan acquisitions for application to a wide range of disorders affecting the hippocampus.

Materials and methods

MRI acquisition

Several protocol manipulations were required to use a readily available standard single-shot 2D EPI sequence at 3T to produce high spatial resolution images (1 x 1 x 1 mm^3) of the human hippocampus in a short scan time. Rather than whole-brain coverage, a thin slab of twenty 1 mm axial-oblique slices oriented along the long axis of the hippocampus (Fig. 1A) was acquired to yield efficient coverage of bilateral hippocampus with far fewer slices (and thus a significant savings in scan time) than would otherwise be required for whole brain coverage or coverage of the hippocampus using coronal slices as is typical of T2-weighted imaging. Twenty slices was estimated to provide adequate coverage of the bilateral hippocampi in a range of subjects with varying hippocampal volumes while allowing for some asymmetry of bilateral orientation. In addition to providing efficient coverage of the anatomy of interest, fewer total slices enabled a shorter repetition time (TR) that allows for acquisition of more diffusion images per slice per unit time to help overcome the very low signal-to-noise ratio (SNR) (Fig. 1B). A lower than typical b-value of 500 s/mm^2 (versus 1000–1500 s/mm^2) was chosen to further mitigate SNR loss from diffusion weighting (i.e. 67% of b0 signal with b500 relative to 45% at b1000 or 30% at b1500 for a typical brain diffusion coefficient of 0.8×10^{-3} mm^2/s), while still yielding sufficient diffusion contrast (e.g. nulled CSF). The shorter gradient pulses needed for b = 500 s/mm^2 also yielded a shorter echo time (TE), limiting T2 signal loss.

Experiments were performed with a 64 channel RF coil on a 3T Siemens Prisma with 80 mT/m gradient strength per axis which further enable a much shorter TE for a given b value. Diffusion scans were aligned along the long-axis of the hippocampus on high resolution T1-

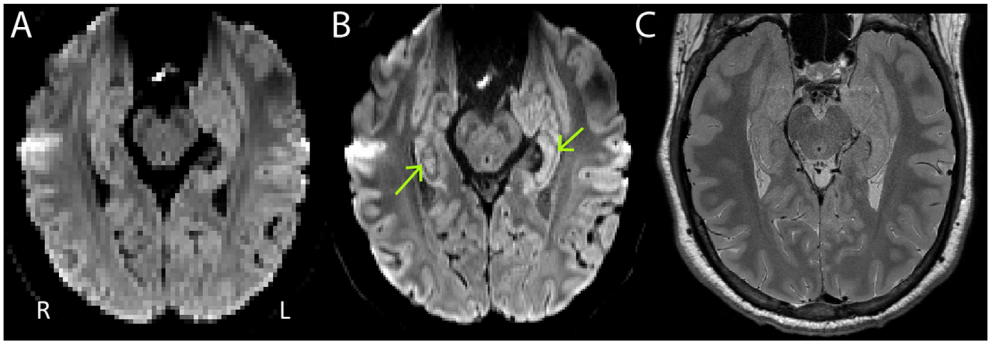

Fig. 2. The axial mean diffusion weighted image (average of 128 b = 500 s/mm^2 DWIs) of a single slice for a healthy 30 year old male is shown for (A) $2 \times 2 \times 2 = 8$ mm^3 resolution and (B) $1 \times 1 \times 1 = 1$ mm^3 resolution. The 1 x 1 x 1 mm^3 6 min acquisition provides an 8-fold increase in spatial resolution, allowing visualization of hippocampal substructure (e.g. SLM, indicated with arrows) that is not appreciable in the 2 mm isotropic scan. (C) The same slice in a conventional fast spin echo 1 x 1 x 1 mm^3 T2-weighted scan (20 slices; TR = 5440 ms, TE = 52 ms) shows excellent grey-white contrast but less delineation of structure within the hippocampus relative to the DWI.

weighted MPRAGE ($0.85 \times 0.85 \times 0.85$ mm^3; 3:37 min). Diffusion images were acquired via single shot 2D EPI (GRAPPA R = 2; 6/8 PPF; A/P phase encode), FOV = 220×216 mm^2, matrix = 220×216, BW=1420 Hz/px, 20 1 mm slices with no gap, 1 x 1 x 1 mm^3 with no interpolation, TE = 72 ms, TR = 2800 ms, diffusion time = 29 ms, b = 500 s/mm^2 with variable monopolar gradient directions and averages as listed below, and 12 b = 0 s/mm^2. Pre-scan normalize was used to correct for the marked B1-inhomogeneity across the slice (given the 64 channel head coil) for better visualization of the hippocampus; comparisons to non-normalized data showed no difference in tensor parameter quantification but far poorer visualization of the hippocampus (data not shown). Note that simultaneous multi-slice (SMS, multi-band) would have provided further time savings to permit more scans, but was not used here as it did not yield adequate image quality even with an acceleration factor of 2, presumably due to the small slab of closely spaced slices.

In order to develop a hippocampus diffusion method that could be readily incorporated into a brain MRI protocol involving other scans for wide applicability to clinical studies, we aimed for a ~6 min acquisition time. On the Prisma, 6 min enables the acquisition of about 128 diffusion weighted images per slice at 1 x 1 x 1 mm^3, with a 10:1 ratio of DWIs to b0s. SNR of the single DWIs was measured as 3–5 in the hippocampus, and 6–8 in the cortex closer to the 64 channel head coil elements. Given the known improvement in SNR afforded by taking multiple signal averages, a sub-study was carried out to test the effect of the number of diffusion encoding directions versus averages (while maintaining a roughly equal total number of DWIs and total scan time). The following scans were acquired at 1 x 1 x 1 mm^3 resolution in a single session on four 30–34 year old healthy right handed adults (3 males; 1 female): 128 directions x 1 average, 64 directions x 2 averages, 30 directions x 4 averages, 20 directions x 6 averages, 10 directions x 12 averages; each with an acquisition time of 6:20–6:45 min. In addition, a 2 x 2 x 2 mm^3 128 direction single average diffusion protocol (with matched TE and TR as the main acquisition described here) was acquired in each subject to provide a high-SNR baseline 'ground truth' comparison for the diffusion parameters. Total scan time was ~44 min. All subjects gave written informed consent and were screened for contraindications to MRI prior to participation. This study was approved by the Health Research Ethics Board at the University of Alberta.

Image processing and region-of-interest analysis

ExploreDTI v4.8.6 (Leemans et al., 2009) was used to process the diffusion data including Gibbs ringing/motion/distortion correction and tensor calculation with ordinary linear least squares. Note that the default parameter to "clean up physically implausible signal" (Perrone et al., 2015) was turned off as it is optimized for data with SNR of 15–30 and has the potential for bias when applied to this data (SNR ~3–5). In cases with more than 1 average, the individual magnitude images of repeated directions were averaged (Matlab 2015b) prior to tensor calculation. The effects of the number of gradient directions versus averages on FA and MD was evaluated in four core tissue classes: white matter (central portions of the splenium), cerebrospinal fluid (lateral ventricles), temporal cortical grey matter and right hippocampus (body, medial to stratum lacunosum-moleculare), with manually drawn 2D regions-of-interest (ROIs). Repeated-measures ANOVA was used to determine within-subject differences in FA or MD across acquisitions for each ROI, with a p-value threshold of <0.05.

Hippocampal segmentation

As a proof of principle, hippocampal subfields were manually segmented directly on the mean diffusion weighted images of the 10 direction, 12 average acquisition for each subject by a trained user (author TS). The hippocampus was divided into the head, body and tail according to body ranging rules (Wisse et al., 2017), and the body was further subdivided into cornu ammonis (CA) 1–3, stratum lacunosum moleculare (SLM) and CA4/dentate gyrus. Segmentations were performed separately in each hemisphere. FA and MD were then extracted from each 3D subfield ROI. Omnibus differences in FA and MD between subfields were determined with one-way ANOVA and followed with pairwise comparisons at a p-value threshold of 0.05. Paired t-tests were used to test for hemispheric differences in FA or MD of each subfield.

Results

Visualization of hippocampal structure on high resolution DWI

For all acquisitions, there was marked improvement in the visualization and contrast within the hippocampus on the mean DWI images at 1 mm isotropic relative to both 'standard resolution' 2 mm isotropic diffusion scans and conventional T2-weighted scans at 1 mm isotropic (Fig. 2). As seen in Fig. 3 over multiple slices, the 1 mm DWI resolution allows impressive visualization of hippocampal internal architecture in the head, body and tail. The hippocampal head is well delimited from the amygdala in the axial plane. The SLM is clearly visualized along the longitudinal axis of the hippocampus in both the axial and coronal planes. The hippocampal digitations are easily seen given the enhanced contrast within the hippocampus and exterior border given the lack of CSF signal from diffusion weighting. Remarkable variability in overall shape and degree of digitations can be seen between individuals even among four healthy adults of similar age in their early 30s (Fig. 4), while all show similar image contrast and visualization of the SLM throughout the entire structure for all subjects.

The primary diffusion tensor direction suggests variable microstructural organization across a single axial-oblique slice of the hippocampus (Fig. 4). A higher proportion of anterior-posterior (green) orientations can be seen in the tail, along with a cluster of left-right (red) orientations in the medial portion of the body, and scattered regions with inferior-superior (blue) orientations in the head that is present in 3 of 4 subjects (albeit noting the limitations of comparing a single slice across

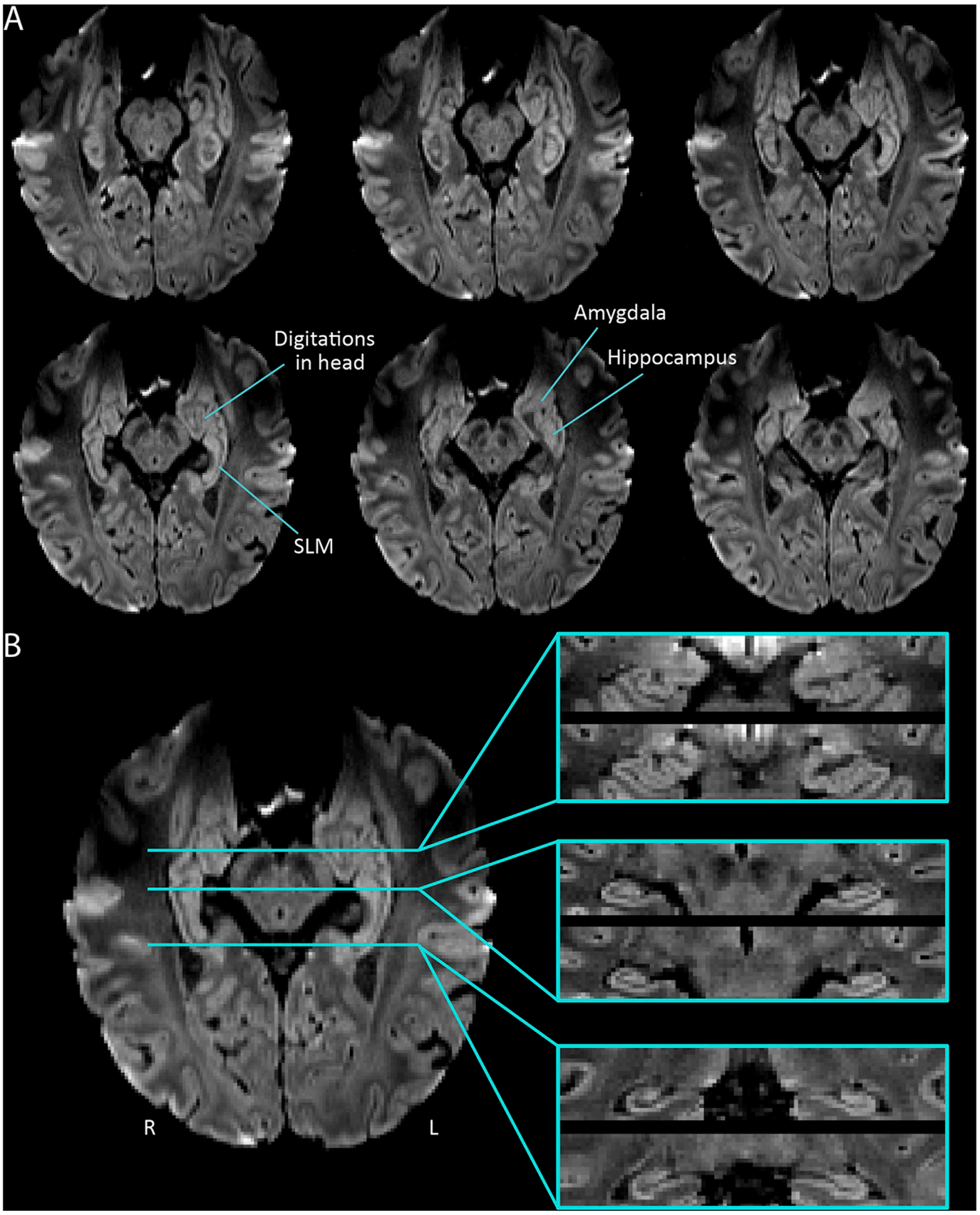

Fig. 3. Mean diffusion weighted images (average of 120 b = 500 s/mm^2 DWIs) with 1 mm isotropic spatial resolution acquired in 6 min for a healthy 30 year old male showing (A) six sequential axial-oblique slices (inferior to superior) and (B) representative reconstructed coronal sections through the head, body and tail. All views reveal detailed structure within the hippocampus, as well as delineation between the hippocampus and surrounding structures like the amygdala.

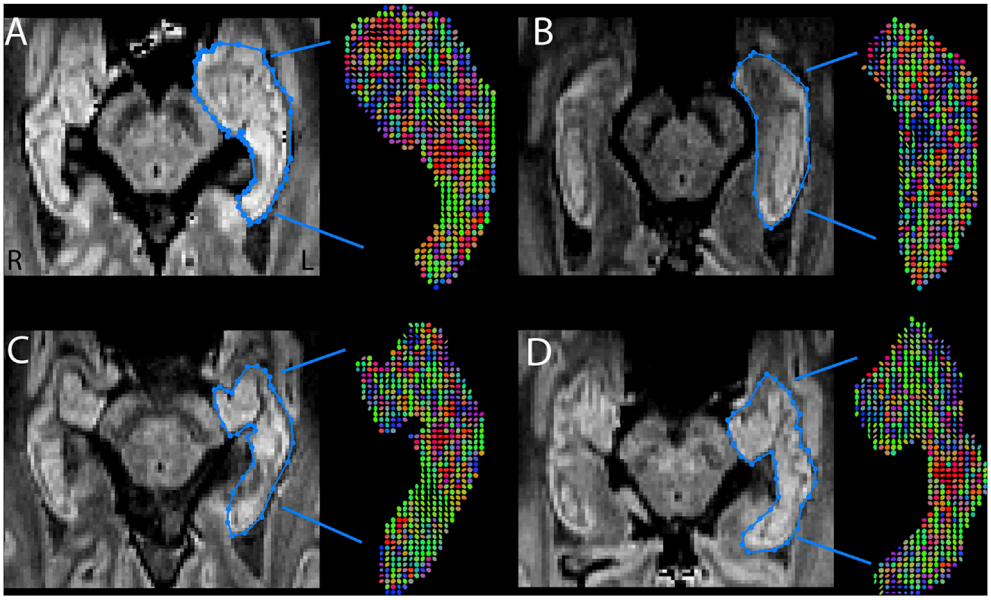

Fig. 4. Mean 1 mm isotropic DWI images and accompanying diffusion ellipsoids (colour coded with primary eigenvector) within the left hippocampus for each of 4 healthy participants: (A) 30 year old male, (B) 34 year old male, (C) 34 year old male, and (D) 33 year old female. Substantial inter-subject variability can be seen for overall hippocampal shape and degree of digitations. The SLM is clearly visualized throughout the entire head, body and tail, and the hippocampus is well delineated from surrounding structures in all participants. Primary diffusion direction (note this is not weighted by FA as in standard colourmap) varies across the hippocampus and between subjects; however, some consistent patterns appear to emerge including a higher proportion of anterior-posterior orientation (green) in the tail, a cluster of left/right orientations (red) in the mid body, and a scattering of inferior-posterior orientations (blue) in the head.

subjects with varying hippocampal shapes).

Directions versus averages

Mean DWI b500 images across the five combinations of diffusion gradient directions and averages for the 1 mm isotropic resolution are visually identical, as expected (Fig. 5 A-E). In addition, colour FA maps (Fig. 5 F-J), FA maps (Fig. 5 K-O) and MD maps (Fig. 5 P-T) are remarkably similar, regardless of the combination of averages and directions. FA and MD values measured from ROIs in the white matter (splenium), cortical grey matter, CSF and hippocampus confirm similar tensor parameter values across acquisitions (Fig. 6). Indeed, repeated measures ANOVA revealed no difference in FA or MD across any of the 1 mm^3 acquisitions with the exception of white matter MD, which was elevated in the 128 direction single average acquisition relative to the other four acquisitions. Likewise, similar values are seen between 1 mm^3 acquisitions and the 'standard' 2 mm isotropic acquisition, with the exception of FA of the hippocampus and GM which are lower in the 2 mm acquisitions likely as a result of partial volume effects in these ROIs at poorer spatial resolution.

Diffusion in hippocampal subfields

As outlined in the Methods, the hippocampus was manually segmented into the head, 3 segments of the body (CA1-3, CA4/dentate gyrus, and SLM), and tail on the mean DWI (Fig. 7A). Over the four healthy young adults, MD values were similar in the head ($0.80 \pm 0.02 \times 10^{-3}$ mm^2/s), body CA1-3 ($0.77 \pm 0.03 \times 10^{-3}$ mm^2/s), body CA4/DG ($0.80 \pm 0.03 \times 10^{-3}$ mm^2/s) and tail regions ($0.80 \pm 0.03 \times 10^{-3}$ mm^2/s), but ANOVA revealed that MD of the body SLM was significantly higher ($0.91 \pm 0.03 \times 10^{-3}$ mm^2/s) than other sub-regions ($p < .001$) (Fig. 7B). FA was similar across the head (0.32 ± 0.03), body CA1-3 (0.32 ± 0.02) and body CA4/DG (0.30 ± 0.02) regions, but was lower in the body SLM (0.26 ± 0.01; $p < .001$) and higher in the tail (0.34 ± 0.02; $p < .001$ to 0.015) (Fig. 7C). There was no significant hemispheric asymmetry of FA or MD for any subfield.

Discussion

This 3T study demonstrates the feasibility of acquiring high resolution (1 mm isotropic) diffusion images of the hippocampus in a clinically applicable scan time of 6 min, and may have major implications for the study of a range of neurological and psychiatric disorders. These images reveal impressive detail of hippocampal substructure, in particular delineation of the SLM, digitations in the head, and differentiation of the hippocampus from surrounding structures such as the amygdala that are impossible to visualize with the typical resolution (>2 mm isotropic) diffusion protocols used almost exclusively in previous literature. Indeed, the unique contrast offered by mean diffusion weighted images, which include both diffusion weighting and T2 weighting, is less apparent at lower spatial resolution given partial volume effects among hippocampal subfields and between the hippocampus and surrounding tissues/CSF. Here we demonstrate the potential to use high resolution diffusion images to segment hippocampal subfields directly on these native space diffusion images without co-registration to another high resolution scan (T1 or T2), allowing quantification of diffusion parameters which may provide localization of tissue pathology in disease.

The protocol presented here can be readily applied without custom pulse programs since it is based on widely available single-shot 2D EPI, but it did require several specific modifications (relative to a typical low resolution whole brain protocol) that together can offset some of the marked SNR loss in going to 1 mm isotropic resolution. Specifically, a small slab of twenty 1 mm axial-oblique slices aligned along the length of the hippocampus was used to limit the number of slices needed to get full coverage of the hippocampus; while the 1 mm isotropic images are still easily viewed in other planes as shown in Fig. 3B. The limited slices also enables a reduction of TR (2.8 s here), thus enabling more scans per unit time for each slice; in our case 120–128 DWIs were acquired per slice over 6 min in the 1 mm isotropic protocols, whereas conventional whole brain 2 mm isotropic with many more slices might acquire 30–60 DWI per slice in that same time. Image quality was further aided by the use of a 64 channel head RF coil and the 80 mT/m per axis gradient strength, which enabled relatively short TE (72 ms) to minimize T2 signal loss, even with a long readout train. In addition, a lower than typical b value of 500 s/mm^2 was chosen to mitigate signal loss (a low b value also limits TE) while still yielding adequate diffusion weighted contrast within the hippocampus.

The 1 mm isotropic dataset produced high-quality mean DWIs with excellent visualization of hippocampal structure (Fig. 3). A substantial degree of inter-subject variability is seen in overall hippocampal shape, internal architecture and degree of digitation among these 4 healthy adults in their early 30s (Fig. 4). Although the relevance of this variability is unknown, it points to the sensitivity of this approach for examining

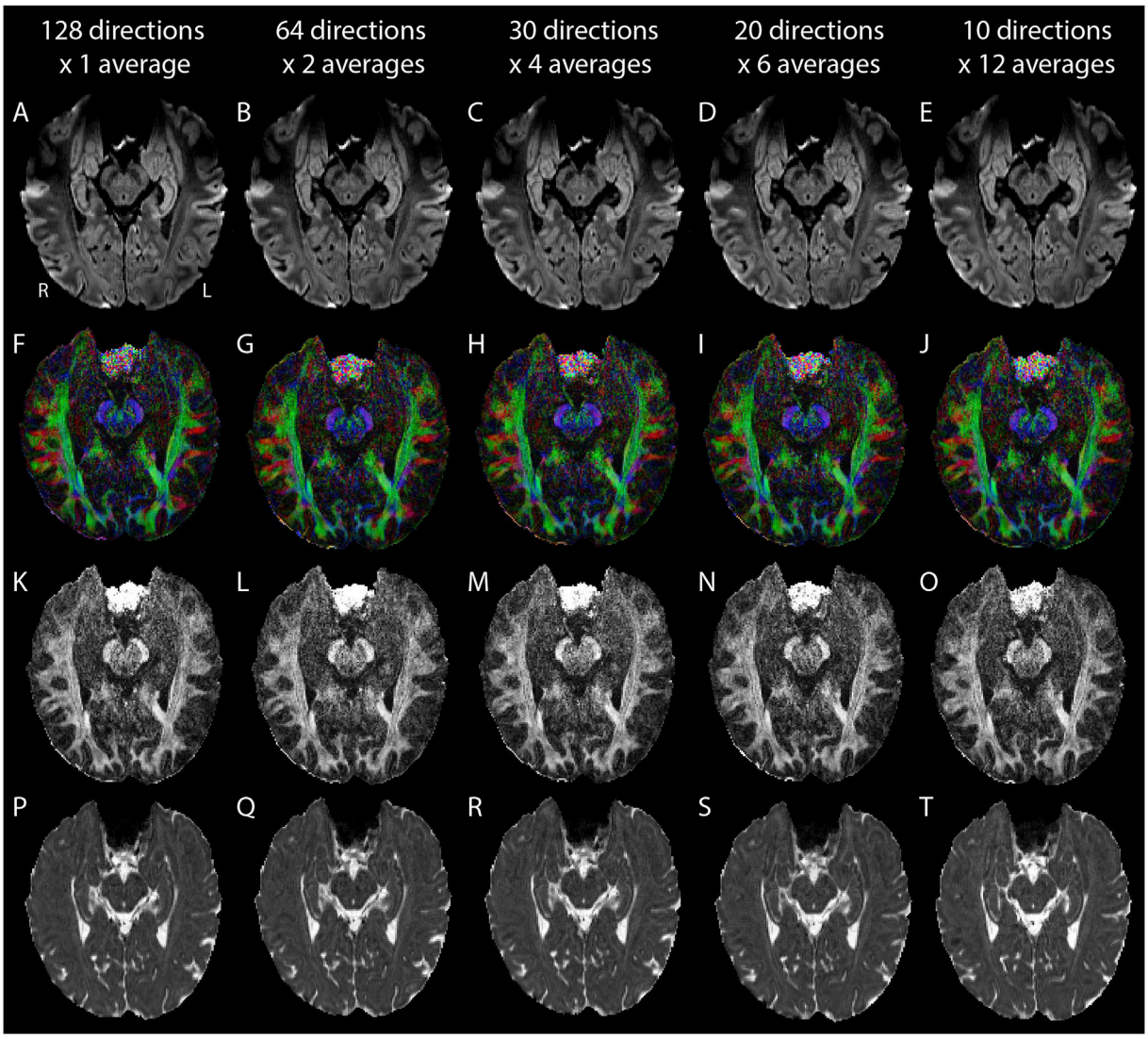

Fig. 5. (A–E) Mean 1 mm isotropic diffusion weighted images ($b = 500\ s/mm^2$), (F–J) FA colour maps, (K–O) FA maps and (P–T) MD maps of a 30 year old male for each of the five acquisitions (listed across the top). Nearly identical contrast is seen in the mean DWI for each acquisition, as expected as they are the average of 120–128 DWIs. Likewise, similar quality parameter maps are produced by all 5 acquisitions, suggesting minimal differences from acquiring a greater number of diffusion encoding directions relative to fewer directions but greater averages.

hippocampal morphology in addition to diffusion parameters suggestive of its microstructure. Evaluation of primary diffusion vectors shows some regional consistency between subjects (Fig. 4), e.g. a cluster of left-right orientations (red) in the body that are fairly consistent across 3 of the 4 subjects whom have similarly shaped hippocampi. This may comprise part of the perforant pathway connecting the entorhinal cortex to the dentate gyrus, which has been previously delineated with DTI tractography in *ex-vivo* human hippocampus samples (Augustinack et al., 2010). Mixed fibre orientations seen within the SLM have also been noted previously in *ex-vivo* work (Coras et al., 2014), and a higher proportion of anterior-posterior projections observed in the tail may reflect a confluence of axons leading into the fimbria fornix. Future work will examine the degree to which structural variability (e.g. number of digitations) relates to cognition and disorders involving alteration of the hippocampus (Oppenheim et al., 1998).

The mean DWIs produced in this protocol provided sufficient contrast for segmentation of gross hippocampal sub-regions directly, without co-registration to other images such as T1 and T2 as required in previous literature. Segmenting on native space images importantly mitigates the potential for errors from mis-registration given the additional susceptibility and eddy current distortions in EPI, while the higher spatial resolution minimizes partial volume errors that are particularly important to consider for such small structures. Diffusion parameters in hippocampal segmentations were quite consistent across the 4 subjects, with MD values of $0.77–0.80 \times 10^{-3}\ mm^2/s$ in all structures except the SLM, which had consistently higher MD of $0.91 \pm 0.03 \times 10^{-3}\ mm^2/s$. Likewise, FA values were ~0.30–0.32 for the head, body CA1-3 and body CA4/DG regions, but was lower in the SLM (0.26) and higher in the tail (0.34). Although the SLM is partly composed of white matter, it is a molecular layer with less consistent fibre orientation than typical cortical white matter, likely leading to lower FA here. Interestingly, our finding of increased MD and reduced FA in the SLM contradicts previous *ex-vivo* work finding lower MD and higher FA in this structure than surrounding hippocampal regions (Shepherd et al., 2007); however, this same study demonstrated a reduction in the consistency of fibre orientation in the SLM relative to surrounding tissues. Specifically, the authors note that apical dendrites diverge orthogonally within the SLM, which may suggest a complexity of fibre orientation within the SLM that cannot be appreciated at a macroscopic scale (i.e. in going from 0.007 mm^3 voxels *ex-vivo* to 1 mm^3 voxels *in-vivo* here). Conversely, large pyramidal neurons in

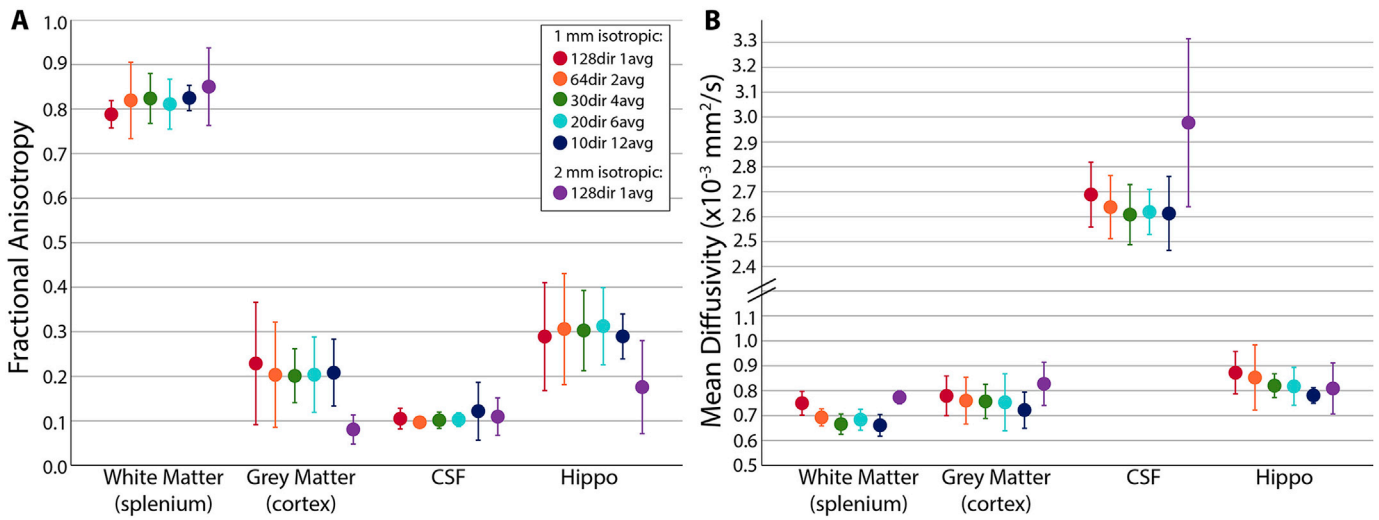

Fig. 6. Mean and standard deviation of (A) FA and (B) MD over the 4 participants in 4 ROIs across 6 acquisitions that vary gradient directions and averages (the first five are 1 mm isotropic resolution and the last one is 2 mm isotropic). Repeated Measures ANOVA revealed no difference in FA and MD values across 1 mm^3 acquisitions, with the exception of white matter MD which was higher in the 128 direction x 1 average acquisition than all other combinations of directions and averages. Lower FA in both CSF and hippocampus ROIs in the 2 mm acquisition likely stems from partial volume effects at this lower resolution which are less apparent in white matter or CSF in the ventricles.

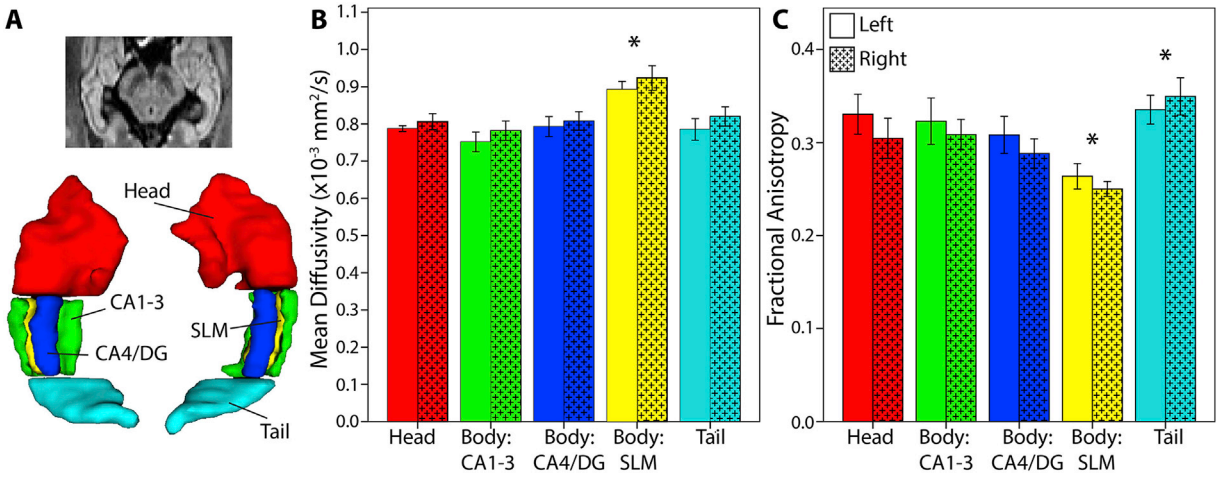

Fig. 7. (A) Example of a 3D reconstruction of a hippocampal subfield segmentation for a single subject that was performed by an experienced user (author TS) directly on mean 1 mm isotropic DWI images (10 direction, 12 average). The hippocampus was divided into the head, body and tail, and the body was further subdivided into CA1-3, CA4/DG, and SLM. (B) In the four healthy controls, similar MD values of ~0.80×10^{-3} mm^2/s are seen across all structures except the body SLM, which has significantly higher MD at ~0.91×10^{-3} mm^2/s. (C) The head, body CA1-3 and body CA4/DG regions all have similar FA values around ~0.32 in all 4 participants, whereas the body SLM has significantly lower FA of ~0.26 and the tail has significantly higher FA at ~0.34. There were no significant differences between left and right values for MD or FA in any region.

CA1-3 exhibit radial fibre orientation that may be conserved even at a coarser scale.

A consistent and homogenous pattern of FA and MD across the remaining sub-regions among healthy subjects may prove advantageous for identifying localized areas of pathology (as does homogenous MD across the brain for acute stroke detection, for example). A large body of previous work using low spatial resolution diffusion protocols has indicated that FA and MD in the hippocampus are sensitive to pathological change, demonstrating transient changes in these parameters associated with a range of acute neurological conditions (Bartsch et al., 2015) as well as long term changes associated with healthy aging (e.g. Carlesimo et al., 2010) and a range of chronic neurological conditions such as epilepsy (e.g. Nazem-Zadeh et al., 2014) and Alzheimer's Disease (e.g. Hong et al., 2013; Tang et al., 2016), among many others. Diffusion parameter alterations may suggest changes in extracellular volume, membrane permeability, myelin integrity and other microstructural components of hippocampal degradation associated with these disorders, even if these methods are unable to tease apart or specify the underlying cellular mechanisms. Although informative, all of this previous work has been at low spatial resolution, which limits accurate localization of diffusion abnormalities, and is prone to partial volume effects that could be lessened with high resolution protocols such as the one proposed here. Moreover, it is well established that specific hippocampal regions, in particular CA1 subfields, appear to be selectively sensitive to cellular damage from ischemia, hypoglycemia and other insults (Schmidtkastner and Freund, 1991). Likewise, many disorders have been associated with sub-field specific pathology, e.g. cellular loss in CA1 in epilepsy (Steve et al., 2014), that suggests a need to better localize diffusion tensor parameter changes with higher resolution protocols.

A critical challenge of high spatial resolution diffusion MRI is the very low SNR of the individual raw diffusion images. Averaging was tested as a means to increase SNR at this high resolution, given the low SNR of

individual un-averaged images going into the tensor (Fig. 1B) despite the signal boosting strategies used here (lower b-value, short TE, etc.); however, averaging was not shown to be of benefit. Visual inspection of the resulting parameter maps and FA/MD measurements from various ROIs did not uncover any appreciable differences between these various averages/gradient direction approaches. One potential problem with the 10 direction, 12 average method is the summation of magnitude images which has the potential to create bias from Rician noise; however, this does not appear to be a major issue given that the FA and MD values in white matter produced by our 10 direction, 12 average 1 mm isotropic images were very similar to that of the 128 direction, single average higher SNR 2 mm isotropic images which were not averaged. Ideally the complex images would be averaged to avoid enhancing the noise floor, but correcting for shot-to-shot phase variations is problematic in diffusion images. Extracting the 'real' images from the complex data appears advantageous for low SNR diffusion data in human brain (Eichner et al., 2015); however, these methods are not readily available. The relationship between noise and diffusion tensor analysis is complex (Anderson, 2001; Andersson, 2008; Jones and Basser, 2004; Pierpaoli and Basser, 1996) and is beyond the scope of the current paper. Future work will look at other tensor algorithms and de-noising strategies (St-Jean et al., 2016; Veraart et al., 2016), to see if tensor quantification can be improved to further shorten scan time or allow higher angular resolution within a constrained scan time.

The use of single-shot EPI with parallel imaging has the advantage of enabling straightforward implementation on a range of scanners without the need for custom methods. Single-shot EPI is widely used for diffusion acquisitions, including in advanced custom acquisitions such as the Human Connectome Project with high resolution (1.25 mm isotropic) multi-shell high b-value whole brain diffusion data (Sotiropoulos et al., 2013). Beyond single-shot EPI, several groups have aimed to push high spatial resolution (1 mm isotropic has been a target) with other diffusion acquisition methods based on 3D multi-slabs, reduced field of view and other acceleration factors (Bruce et al., 2017; Heidemann et al., 2012; Wu et al., 2016). Although potentially advantageous, scan times are still 30–60 min even at 7T, and these complex acquisitions may be more difficult to implement widely on clinical systems. Another novel method using simultaneous multi-slab acquisition with Connectome gradients reported 0.66–0.76 mm isotropic resolution over the whole brain *in vivo* with either 64 directions, 4 averages at b = 1500 s/mm^2 in 100 min, or 128 directions, 1 average at b = 1800 s/mm^2 in 50 min (Setsompop et al., 2018). This example again requires longer scan time; however, more focused application of these methods to single slabs may make them feasible for very high resolution study of the hippocampus.

The low b-value of 500 s/mm^2 prohibits the use of more complex diffusion processing algorithms aimed at disentangling crossing fibre microstructure *in-vivo*, which is observed in the hippocampus in *ex-vivo* data (Colon-Perez et al., 2015; Coras et al., 2014; Modo et al., 2016; Shepherd et al., 2007). One recent study has used high angular resolution, high b-value diffusion spectrum acquisition to visualize hippocampal white matter networks, though at both low spatial resolution (2.2 mm isotropic) and at the cost of a 43 min diffusion sequence (Wei et al., 2017) which is of limited clinical applicability for most patient populations. High b-value, high angular resolution protocols will necessarily require a compromise of resolution or scan time relative to the protocol proposed here. As a post-hoc analysis, the effect of b-value was evaluated on 1 mm isotropic DTI in two subjects by acquiring 10 directions and 10 averages at b = 500, 750 and 1000 s/mm^2. The two higher b value acquisitions yielded similar visualization of the hippocampus and similar contrast on FA and MD maps as b = 500 s/mm^2, albeit with slightly lower FA and MD values (data not shown). Thus, 1 mm isotropic acquisitions with higher b-values are likely feasible but presumably will require longer scan times to recover SNR. As always, the effect of b value and other acquisition parameters on the absolute value of diffusion parameters should be considered when comparing datasets.

This study presents a practical and readily available approach for the acquisition of high spatial resolution diffusion tensor images of the human hippocampus in a clinically feasible scan time at 3T. The 1 mm isotropic mean DWIs reveal impressive contrast and detail of hippocampal substructure that differs between individuals and allows for segmentation of subfields directly, without co-registration to other imaging modalities. Diffusion parameters within the hippocampus appear to be fairly consistent across sub-regions (with the exception of the SLM and tail) but are expected to differ in pathology as suggested by previous literature identifying FA and MD abnormalities in the hippocampus with lower resolution acquisitions. This method has the potential to impact the study of healthy development, aging, and numerous disorders affecting the hippocampus by providing the necessary spatial resolution (1 mm isotropic) to measure diffusion parameters in distinct hippocampal sub-regions in 6 min or less.

Acknowledgments

Operating grant was provided by the Canadian Institutes of Health Research. Author CB acknowledges a salary award from the Canada Research Chair (Tier 1) program. Infrastructure was provided by the Canada Foundation for Innovation, Alberta Innovation and Advanced Education, and the University Hospital Foundation.

References

Anderson, A.W., 2001. Theoretical analysis of the effects of noise on diffusion tensor imaging. Magn. Reson. Med. 46, 1174–1188.
Andersson, J.L., 2008. Maximum a posteriori estimation of diffusion tensor parameters using a Rician noise model: why, how and but. Neuroimage 42, 1340–1356.
Augustinack, J.C., Helmer, K., Huber, K.E., Kakunoori, S., Zollei, L., Fischl, B., 2010. Direct visualization of the perforant pathway in the human brain with ex vivo diffusion tensor imaging. Front. Hum. Neurosci. 4, 42.
Barbagallo, G., Nicoletti, G., Cherubini, A., Trotta, M., Tallarico, T., Chiriaco, C., Nistico, R., Salvino, D., Bono, F., Valentino, P., Quattrone, A., 2014. Diffusion tensor MRI changes in gray structures of the frontal-subcortical circuits in amyotrophic lateral sclerosis. Neurol. Sci. 35, 911–918.
Barth, C., Steele, C.J., Mueller, K., Rekkas, V.P., Arelin, K., Pampel, A., Burmann, I., Kratzsch, J., Villringer, A., Sacher, J., 2016. In-vivo dynamics of the human Hippocampus across the menstrual cycle. Sci. Rep. 6, 32833.
Bartsch, T., Dohring, J., Reuter, S., Finke, C., Rohr, A., Brauer, H., Deuschl, G., Jansen, O., 2015. Selective neuronal vulnerability of human hippocampal CA1 neurons: lesion evolution, temporal course, and pattern of hippocampal damage in diffusion-weighted MR imaging. J. Cerebr. Blood Flow Metabol. 35, 1836–1845.
Bernhardt, B.C., Bernasconi, A., Liu, M., Hong, S.J., Caldairou, B., Goubran, M., Guiot, M.C., Hall, J., Bernasconi, N., 2016. The spectrum of structural and functional imaging abnormalities in temporal lobe epilepsy. Ann. Neurol. 80, 142–153.
Bruce, I.P., Chang, H.C., Petty, C., Chen, N.K., Song, A.W., 2017. 3D-MB-MUSE: a robust 3D multi-slab, multi-band and multi-shot reconstruction approach for ultrahigh resolution diffusion MRI. Neuroimage 159, 46–56.
Cappellani, R., Bergsland, N., Weinstock-Guttman, B., Kennedy, C., Carl, E., Ramasamy, D.P., Hagemeier, J., Dwyer, M.G., Patti, F., Zivadinov, R., 2014. Subcortical deep gray matter pathology in patients with multiple sclerosis is associated with white matter lesion burden and atrophy but not with cortical atrophy: a diffusion tensor MRI study. AJNR Am. J. Neuroradiol. 35, 912–919.
Carlesimo, G.A., Cherubini, A., Caltagirone, C., Spalletta, G., 2010. Hippocampal mean diffusivity and memory in healthy elderly individuals: a cross-sectional study. Neurology 74, 194–200.
Cha, J., Greenberg, T., Song, I., Blair Simpson, H., Posner, J., Mujica-Parodi, L.R., 2016. Abnormal hippocampal structure and function in clinical anxiety and comorbid depression. Hippocampus 26, 545–553.
Cherubini, A., Peran, P., Caltagirone, C., Sabatini, U., Spalletta, G., 2009. Aging of subcortical nuclei: microstructural, mineralization and atrophy modifications measured in vivo using MRI. Neuroimage 48, 29–36.
Chiapponi, C., Piras, F., Fagioli, S., Girardi, P., Caltagirone, C., Spalletta, G., 2014. Hippocampus age-related microstructural changes in schizophrenia: a case-control mean diffusivity study. Schizophr. Res. 157, 214–217.
Colon-Perez, L.M., King, M., Parekh, M., Boutzoukas, A., Carmona, E., Couret, M., Klassen, R., Mareci, T.H., Carney, P.R., 2015. High-field magnetic resonance imaging of the human temporal lobe. Neuroimage-Clinical 9, 58–68.
Coras, R., Milesi, G., Zucca, I., Mastropietro, A., Scotti, A., Figini, M., Muhlebner, A., Hess, A., Graf, W., Tringali, G., Blumcke, I., Villani, F., Didato, G., Frassoni, C., Spreafico, R., Garbelli, R., 2014. 7T MRI features in control human hippocampus and hippocampal sclerosis: an ex vivo study with histologic correlations. Epilepsia 55, 2003–2016.
Eichner, C., Cauley, S.F., Cohen-Adad, J., Moller, H.E., Turner, R., Setsompop, K., Wald, L.L., 2015. Real diffusion-weighted MRI enabling true signal averaging and increased diffusion contrast. Neuroimage 122, 373–384.

Heidemann, R.M., Anwander, A., Feiweier, T., Knosche, T.R., Turner, R., 2012. k-space and q-space: combining ultra-high spatial and angular resolution in diffusion imaging using ZOOPPA at 7 T. Neuroimage 60, 967–978.
Hong, Y.J., Yoon, B., Lim, S.C., Shim, Y.S., Kim, J.Y., Ahn, K.J., Han, I.W., Yang, D.W., 2013. Microstructural changes in the hippocampus and posterior cingulate in mild cognitive impairment and Alzheimer's disease: a diffusion tensor imaging study. Neurol. Sci. 34, 1215–1221.
Jackson, G.D., Berkovic, S.F., Duncan, J.S., Connelly, A., 1993. Optimizing the diagnosis of hippocampal sclerosis using MR imaging. AJNR Am. J. Neuroradiol. 14, 753–762.
Jones, D.K., Basser, P.J., 2004. "Squashing peanuts and smashing pumpkins": how noise distorts diffusion-weighted MR data. Magn. Reson. Med. 52, 979–993.
Kliper, E., Ben Assayag, E., Korczyn, A.D., Auriel, E., Shopin, L., Hallevi, H., Shenhar-Tsarfaty, S., Mike, A., Artzi, M., Klovatch, I., Bornstein, N.M., Ben Bashat, D., 2016. Cognitive state following mild stroke: a matter of hippocampal mean diffusivity. Hippocampus 26, 161–169.
Kobe, T., Witte, A.V., Schnelle, A., Grittner, U., Tesky, V.A., Pantel, J., Schuchardt, J.P., Hahn, A., Bohlken, J., Rujescu, D., Floel, A., 2016. Vitamin B-12 concentration, memory performance, and hippocampal structure in patients with mild cognitive impairment. Am. J. Clin. Nutr. 103, 1045–1054.
Leemans, A., Jeurissen, B., Sijbers, J., Jones, D., 2009. ExploreDTI: a graphical toolbox for processing, analyzing, and visualizing diffusion MR data. In: 17th Annual Meeting of International Society of Magnetic Resonance Medicine, Hawaii, USA, 2009, p. 3537.
Li, Y.D., Dong, H.B., Xie, G.M., Zhang, L.J., 2013. Discriminative analysis of mild Alzheimer's disease and normal aging using volume of hippocampal subfields and hippocampal mean diffusivity: an in vivo magnetic resonance imaging study. Am. J. Alzheimer's Dis. Other Dementias 28, 627–633.
Modo, M., Hitchens, T.K., Liu, J.R., Richardson, R.M., 2016. Detection of aberrant hippocampal mossy fiber connections: ex vivo mesoscale diffusion MRI and microtractography with histological validation in a patient with uncontrolled temporal lobe epilepsy. Hum. Brain Mapp. 37, 780–795.
Nazem-Zadeh, M.R., Schwalb, J.M., Elisevich, K.V., Bagher-Ebadian, H., Hamidian, H., Akhondi-Asl, A.R., Jafari-Khouzani, K., Soltanian-Zadeh, H., 2014. Lateralization of temporal lobe epilepsy using a novel uncertainty analysis of MR diffusion in hippocampus, cingulum, and fornix, and hippocampal volume and FLAIR intensity. J. Neurol. Sci. 342, 152–161.
Nazeri, A., Mulsant, B.H., Rajji, T.K., Levesque, M.L., Pipitone, J., Stefanik, L., Shahab, S., Roostaei, T., Wheeler, A.L., Chavez, S., Voineskos, A.N., 2017. Gray matter neuritic microstructure deficits in schizophrenia and bipolar disorder. Biol. Psychiatr. 82, 726–736.
Neunuebel, J.P., Knierim, J.J., 2014. CA3 retrieves coherent representations from degraded input: direct evidence for CA3 pattern completion and dentate gyrus pattern separation. Neuron 81, 416–427.
Oppenheim, C., Dormont, D., Biondi, A., Lehericy, S., Hasboun, D., Clemenceau, S., Baulac, M., Marsault, C., 1998. Loss of digitations of the hippocampal head on high-resolution fast spin-echo MR: a sign of mesial temporal sclerosis. AJNR Am. J. Neuroradiol. 19, 457–463.
Pereira, J.B., Valls-Pedret, C., Ros, E., Palacios, E., Falcon, C., Bargallo, N., Bartres-Faz, D., Wahlund, L.O., Westman, E., Junque, C., 2014. Regional vulnerability of hippocampal subfields to aging measured by structural and diffusion MRI. Hippocampus 24, 403–414.
Perrone, D., Aelterman, J., Pizurica, A., Jeurissen, B., Philips, W., Leemans, A., 2015. The effect of Gibbs ringing artifacts on measures derived from diffusion MRI. Neuroimage 120, 441–455.
Pierpaoli, C., Basser, P.J., 1996. Toward a quantitative assessment of diffusion anisotropy. Magn. Reson. Med. 36, 893–906.
Planche, V., Ruet, A., Coupe, P., Lamargue-Hamel, D., Deloire, M., Pereira, B., Manjon, J.V., Munsch, F., Moscufo, N., Meier, D.S., Guttmann, C.R., Dousset, V., Brochet, B., Tourdias, T., 2017. Hippocampal microstructural damage correlates with memory impairment in clinically isolated syndrome suggestive of multiple sclerosis. Mult. Scler. 23, 1214–1224.
Sagi, Y., Tavor, I., Hofstetter, S., Tzur-Moryosef, S., Blumenfeld-Katzir, T., Assaf, Y., 2012. Learning in the fast lane: new insights into neuroplasticity. Neuron 73, 1195–1203.
Schmidtkastner, R., Freund, T.F., 1991. Selective vulnerability of the Hippocampus in brain ischemia. Neuroscience 40, 599–636.
Setsompop, K., Fan, Q., Stockmann, J., Bilgic, B., Huang, S., Cauley, S.F., Nummenmaa, A., Wang, F., Rathi, Y., Witzel, T., Wald, L.L., 2018. High-resolution in vivo diffusion imaging of the human brain with generalized slice dithered enhanced resolution: simultaneous multislice (gSlider-SMS). Magn. Reson. Med. 79, 141–151.
Shepherd, T.M., Ozarslan, E., Yachnis, A.T., King, M.A., Blackband, S.J., 2007. Diffusion tensor microscopy indicates the cytoarchitectural basis for diffusion anisotropy in the human hippocampus. AJNR Am. J. Neuroradiol. 28, 958–964.
Sotiropoulos, S.N., Jbabdi, S., Xu, J.Q., Andersson, J.L., Moeller, S., Auerbach, E.J., Glasser, M.F., Hernandez, M., Sapiro, G., Jenkinson, M., Feinberg, D.A., Yacoub, E., Lenglet, C., Van Essen, D.C., Ugurbil, K., Behrens, T.E.J., Consortium, W.U.-M.H, 2013. Advances in diffusion MRI acquisition and processing in the human connectome Project. Neuroimage 80, 125–143.
St-Jean, S., Coupe, P., Descoteaux, M., 2016. Non Local Spatial and Angular Matching: enabling higher spatial resolution diffusion MRI datasets through adaptive denoising. Med. Image Anal. 32, 115–130.
Steve, T.A., Jirsch, J.D., Gross, D.W., 2014. Quantification of subfield pathology in hippocampal sclerosis: a systematic review and meta-analysis. Epilepsy Res. 108, 1279–1285.
Tang, X., Qin, Y., Wu, J., Zhang, M., Zhu, W., Miller, M.I., 2016. Shape and diffusion tensor imaging based integrative analysis of the hippocampus and the amygdala in Alzheimer's disease. Magn. Reson. Imaging 34, 1087–1099.
van Uden, I.W., Tuladhar, A.M., van der Holst, H.M., van Leijsen, E.M., van Norden, A.G., de Laat, K.F., Rutten-Jacobs, L.C., Norris, D.G., Claassen, J.A., van Dijk, E.J., Kessels, R.P., de Leeuw, F.E., 2016. Diffusion tensor imaging of the hippocampus predicts the risk of dementia; the RUN DMC study. Hum. Brain Mapp. 37, 327–337.
Veraart, J., Novikov, D.S., Christiaens, D., Ades-Aron, B., Sijbers, J., Fieremans, E., 2016. Denoising of diffusion MRI using random matrix theory. Neuroimage 142, 394–406.
Wei, P.H., Mao, Z.Q., Cong, F., Yeh, F.C., Wang, B., Ling, Z.P., Liang, S.L., Chen, L., Yu, X.G., 2017. In vivo visualization of connections among revised Papez circuit hubs using full q-space diffusion spectrum imaging tractography. Neuroscience 357, 400–410.
West, M.J., Coleman, P.D., Flood, D.G., Troncoso, J.C., 1994. Differences in the pattern of hippocampal neuronal loss in normal ageing and Alzheimer's disease. Lancet 344, 769–772.
Wisse, L.E.M., Daugherty, A.M., Amaral, R.S.C., Berron, D., Carr, V.A., Ekstrom, A.D., Kanel, P., Kerchner, G.A., Mueller, S.G., Pluta, J., Stark, C.E., Steve, T., Wang, L., Yassa, M.A., Yushkevich, P.A., La Joie, R., 2017. A harmonized protocol for medial temporal lobe subfield segmentation: initial results of the 3-tesla protocol for the hippocampal body. Alzheimer's Dementia: J. Alzheimer's Assoc. 12, P631.
Wu, W., Poser, B.A., Douaud, G., Frost, R., In, M.H., Speck, O., Koopmans, P.J., Miller, K.L., 2016. High-resolution diffusion MRI at 7T using a three-dimensional multi-slab acquisition. Neuroimage 143, 1–14.
Yassa, M.A., Mattfeld, A.T., Stark, S.M., Stark, C.E.L., 2011. Age-related memory deficits linked to circuit-specific disruptions in the hippocampus. Proc. Natl. Acad. Sci. U. S. A. 108, 8873–8878.
Zeineh, M.M., Holdsworth, S., Skare, S., Atlas, S.W., Bammer, R., 2012. Ultra-high resolution diffusion tensor imaging of the microscopic pathways of the medial temporal lobe. Neuroimage 62, 2065–2082.